MEMS FABRICATED NANOPORES AND MICROPORES FUNCTIONALIZED WITH CHROMATE-SELECTIVE SOLVENT POLYMERIC MEMBRANE

By

DANIEL C. RIECK

A thesis submitted in partial fulfillment of
the requirements for the degree of

MASTER OF SCIENCE IN CHEMICAL ENGINEERING

WASHINGTON STATE UNIVERSITY
Department of Chemical Engineering

DECEMBER 2008

To the Faculty of Washington State University

The members of the Committee appointed to examine the thesis of DANIEL C. RIECK find it satisfactory and recommend that it be accepted.

_____
Bernard J. Van Wie, Chair

_____
Cornelius F. Ivory

_____
David F. Moffett

_____
Knona C. Liddell

_____
Haluk Beyenal

ACKNOWLEDGEMENTS

I would first, and above all else, like to thank Jesus Christ for his strength and support. Without him, none of this would even be possible; and he was what really made it worthwhile. As the Apostle Paul wrote in his epistle to the Philippians, after all I have seen and done, even still I find there is no greater or more fulfilling purpose than to know and follow after you, Jesus. My appreciation next goes toward my advisor, Dr. Bernard J. Van Wie, for the patient mentoring and numerous development opportunities he provided, and especially for his guidance of this particular work. We shared many productive and enjoyable discussions regarding research and other areas of life, and often times Dr. Van Wie would get his hands wet in the lab to demonstrate equipment or help solve problems. I want to thank Dr. Cornelius F. Ivory for our numerous valuable and enjoyable discussions about Chemical Engineering, Academia, and research, and for the generous support of his lab and students. It has been a pleasure to work with such a high quality group. My thanks to Dr. David F. Moffett and his lab group for including me in their weekly meetings and giving me valuable feedback on my work. I thank Dr. KNona C. Liddell for her valuable insights in scientific writing and discussion pertaining to my work. My thanks go to Dr. Haluk Beyenal, Dr. H. George Rieck, and Alim Dewan and for their insightful discussion concerning the principles of electrochemical cells. I thank the members of my lab group - Hajime Fuchida, Chris Detzel, Sarah Haarsma, and Natasha Godwin - for the time they invested in helping me with my research and the enjoyable times we had

working side-by-side in the lab. A hearty thanks to Bingwen Liu, who not only provided the micropores in SU-8, but spent some of his valuable time discussing our work and thereby enriching the scientific process. My thanks go to Gary Cheng for providing nanopores in silicon and for his feedback. Finally, I want to thank my immediate family - Robert, Mary, Bennett, and our "adopted brother" Emmanuel Adusei - for their encouragement, sound advice, prayers, and tireless moral support throughout the duration of this work. I am truly blessed to be a member of this family.

MEMS FABRICATED NANOPRES AND MICROPORES FUNCTIONALIZED WITH CHROMATE-SELECTIVE SOLVENT POLYMERIC MEMBRANE

Abstract

By Daniel C. Rieck, M.S.
Washington State University
December 2008

Chair: Bernard J. Van Wie

There is an impetus in the global regulatory industry to develop new monitoring technologies targeting pollutants such as chromate, since current practice requires using expensive technologies such as inductively coupled plasma-mass spectroscopy, and is therefore labor intensive and time-consuming. The Ion Selective Electrode (ISE) is a technology that, despite its numerous benefits, has not been adapted to regulatory monitoring of heavy metals because of its shortcomings in sensitivity and selectivity. One approach to solving this problem is to combine miniaturized ISEs with lab-on-a-chip preconcentration and preseparation technologies. In this thesis, I present a manuscript submitted for publication in Sensors and Actuators B: Chemical that treats fabrication methods for producing nano- and micro-sized chromate-selective ISEs compatible with such lab-on-a-chip separation technology; characterizes these sensors; and compares their function to coated wire electrodes. We used UV lithography and focused ion beam to make single micropores in SU-8 photoresist and nanopores in Si_3N_4 thin films, respectively, functionalizing them with solvent polymeric membrane. We used a membrane formulation consisting of 7.7:62.2:31.1 wt % Aliquat336:2-NPOE:PVC. Our coated wire electrode arrays exhibited a response slope of -61.7 ± 2.4 mV decade^{-1}, limit of detection

(LOD) of 3.0×10^{-6}, and potentiometric selectivity coefficients ranging from 1.3×10^{-2} for SCN^- to 5.0×10^{-5} for SO_3^{2-}. A nano-scale ISE 100 nm in diameter achieved a response slope of -65.2 ± 4.1 mV decade^{-1} and a LOD of 1.8×10^{-5} M, versus -58.6 ± 5.6 mV decade^{-1} and 2.1×10^{-5} for a micro-scale ISE 30 μm in diameter. Response times averaged 29 s for the nano-scale ISE and 40 s for the micro-scale ISE. Electrical resistance measurements demonstrated working ranges of GΩ for the micro-scale ISEs and up to TΩ for the nano-scale ISEs. Predicted pore diameters based on these measurements showed -3% and +18% agreements with actual diameters for a 100 nm nanopore and a 30 μm micropore, respectively. Atomic force microscopy imaging of the micro-scale ISE revealed a properly formed micropore and cast membrane, with exposed membrane diameter exceeding that of the pore opening by 1.7 times. AFM was found to be incapable of distinguishing nano-scale ISEs from Si_3N_4 thin film surface features and dust particles.

TABLE OF CONTENTS

LIST OF TABLES

LIST OF FIGURES

CHAPTER ONE

GENERAL INTRODUCTION

Chromium(VI), the hazardous counterpart to chromium(III), still poses a serious risk to global human and environmental health. Chromium(VI) has been shown to be toxic, mutagenic, carcinogenic, and extremely hazardous to aquatic ecosystems, while chromium(III) has been established as a trace element essential for human health. There was some question as to the extent of the carcinogenic effect of chromium(VI) in various forms [1, 2], but it was shown recently that chromium(VI) from any source has carcinogenic effect when ingested as a component of drinking water [3]. Regulating it is complicated because chromium(VI) and chromium(III) have the ability to readily interconvert [4], though this process favors chromium(VI) reduction [5]. For example, oxidation of chromium(III) into chromium(VI) is possible in soil, but manganese oxide deposits are required as oxidizing agents for this to occur [6]. In contrast, the biosphere is reducing for chromium(VI) and chromium(III) is relatively immobile, so there is little bioconcentration or biomagnification of the pollutant [5]. Nevertheless, chromate pollution at problem sites can remain at serious and persistent levels without remediation efforts [5, 6].

Major sources of chromium(VI) pollution include chromite mining, leather tanning, and industrial runoff. The fate of chromium(VI) in the environment is such that it can accumulate in groundwater, sediment through sorption, and landfills. Problem spots in the U.S. for chromate pollution include New Jersey, which historically was a major site for chromite processing [6]; and California, where chromate pollution exceeding regulated levels has been detected in groundwater. Finally, there are serious chromate pollution problems in India because of its

heavy use in the tanning industry [7], discharges from ship demolition, and poorly regulated dumping of industrial waste. One unique instance of chromium(VI) pollution is found in Washington, specifically the mixed radioactive waste found at the Hanford site where chromate comprises a significant waste fraction and can cause problems with treatment of high level radioactive waste [8].

Though established protocols are available for addressing such problems with chromium(VI) pollution, monitoring and remediation of chromium(VI) is difficult because of its complex and dynamic chemistry in the field [4, 5]. It is easy to alter the oxidation state of chromium when handling samples during analytical procedures, such as when digesting or extracting sample [5]. Hence accepted practice for monitoring chromium requires carefully taking samples in the field and returning them to the laboratory, where expensive, highly technical, and labor intensive analysis is performed using technologies such as Inductively Coupled Plasma-Mass Spectroscopy (ICP-MS) and Atomic Absorption Spectroscopy (AAS) [7, 9]. This has given rise to an impetus in the global regulatory industry to develop new monitoring technologies, with several groups targeting Ion Selective Electrodes (ISEs) as an attractive alternative [7, 9-14]. ISEs sensitive for chromium ions are being particularly sought after as a low-cost, convenient, on-line method of analysis, with hopes of using them for routine analysis of large numbers of data sets [7, 11, 13].

Unfortunately, ISEs have traditionally suffered from limitations in their sensitivity and selectivity that preclude them from widespread adoption by the regulatory industry [15]. The best reported membrane formulations targeting Chromate have a limit of detection that is just under the Maximum Contaminant Level (MCL) in drinking water of 0.1 ppm enforced by the US EPA [16]. This is unacceptable, since ISEs target only free ions in aqueous media, which may

comprise a very small fraction of the overall quantity of a pollutant that is distributed throughout a polluted site [5, 17, 18]. This problem is compounded by the fact that real world samples will also have significant levels of interferents, the identity and levels of which are not always known, making the use of traditional ISEs as trace level analysis tools on any practical level even more improbable.

There is still hope for the ISE, however, because of recent breakthroughs in understanding the theoretical underpinnings of the detection limit of an ISE [15, 17-19]. These studies have led to considerable advances in extending the typical linear range of ISEs; for example, nanomolar detection limits have been achieved for 19 different solvent polymeric membrane formulations for 10 different analytes [18]. The benefits from this design approach include an unprecedented enhancement of their potentiometric selectivities by several orders of magnitude [15]. Unfortunately even these strides forward are unable to address some of the engineering problems posed by real world samples. For example, salt levels in seawater are at high enough levels to cause interferences that mask detectability when trying to measure trace levels of any pollutant, even for enhanced ISEs. Hence such improvements to the lower LOD and selectivity of an ISE alone are not adequate for revolutionizing the regulatory industry.

One parallel approach to enhancing ISE function as a trace-level analysis tool is to combine miniaturized ISEs with powerful lab-on-a-chip preconcentration and preseparation technologies. For example, isotachophoresis (ITP) has been shown to preconcentrate a protein sample starting in the femtomolar range by nearly a million fold, and can effectively separate ionic samples at the same time [20]. ITP is extremely tunable, such that for aqueous samples containing inorganic ions ITP can be used to both effectively separate trace-level interferents and remove high abundance background interferents. Integrating ISEs with ITP has not yet been

accomplished, and from the recent advances in the ISE field this approach emerges as an extremely promising alternative for conducting trace-level analysis. Before this can be realized, miniaturized ISEs implemented in a format compatible with lab-on-a-chip design are needed.

This thesis constitutes a publishable manuscript prepared for submission to *Sensors and Actuators B: Chemical*, in which we describe a fabrication method for producing nano- and microsized chromate selective ISEs compatible with such lab-on-a-chip separation technology, and we characterize these sensors and compare their function to macroscopic coated wire electrodes. Though the manuscript is attributed to multiple authors, I wrote it in its entirety and was responsible for the majority of the experimentation, both in terms of design and execution, as well as the interpretation of the majority of the experimental results. Therefore, it is more expedient to treat the contributions of other authors listed.

Bong-Jae Park carried out Atomic Force Microscopy (AFM) experiments, as well as assisted me in designing them and interpreting AFM images. Bingwen Liu developed the micropore fabrication procedure and provided micropores for me to use in my experiments. Similarly, Gary J. Cheng developed the nanopore fabrication protocol and provided me with nanopores to use for my experiments. David A. Kidwell provided the potentiometer used for ISE calibration experiments and helped with the interpretation of resistance experiments after reviewing the manuscript and discussing my results with me. David F. Moffett helped me learn how to properly perform Axopatch resistance measurements, and aided me in interpreting ISE performance and electrical results through his review of the manuscript and our discussions. Finally, my advisor Dr. Bernie Van Wie aided me in all aspects of interpreting results and helped me considerably in refining the manuscript for publication.

1. R.E. Albert, Environmental Health Perspectives, 92 (1991) p. 91-92.

2. C. Pellerin S.M. Booker, Environmental Health Perspectives, 108 (2000) p. A 402- A407.

3. National Toxicology Program, Research Triangle Park, NC, NTP TR 546 (2008).

4. S.I. Shupack, Environmental Health Perspectives, 92 (1991) p. 7-11.

5. D.E. Kimbrough, Y. Cohen, A.M. Winer, et al., Critical Reviews in Environmental Science and Technology, 29 (1999) p. 1-46.

6. C.D. Palmer P.R. Wittbrodt, Environmental Health Perspectives, 92 (1991) p. 25-40.

7. A.K. Jain, V.K. Gupta, L.P. Singh, et al., Talanta, 65 (2005) p. 716-721.

8. U.S. Department of Energy, B.M. Rapko J.D. Vienna, National Technical Information Service, Springfield, VA, PNL-14019 (2002).

9. V.K. Gupta, A.K. Jain, P. Kumar, et al., Sensors and Actuators B, 113 (2006).

10. Y.-W. Choi, N. Minoura, S.-H. Moon, Talanta, 66 (2005) p. 1254-1263.

11. M.A. Akl, A.K. Ghoneim, M.H.A. El-Aziz, Electroanalysis, 18 (2006) p. 299-306.

12. M.M. Ardakani, A. Dastanpour, M. Salavati-Niasari, Microchimica Acta, 150 (2005) p. 67-72.

13. M.B. Gholivand F. Sharifpour, Talanta, 60 (2003) p. 707-713.

14. A.K. Singh, A. Panwar, S. Kumar, et al., Analyst, 124 (1999) p. 521-525.

15. T. Sokalski, A. Ceresa, T. Zwickl, et al., J. Am. Chem. Soc., 119 (1997) p. 11347-11348.

16. United States Environmental Protection Agency, Office of Water, EPA 816-F-03-016 (2003).

17. E. Bakker, P. Bühlmann, E. Pretsch, Chemical Reviews, 97 (1997) p. 3083-3132.

18. E. Bakker E. Pretsch, Trends in Analytical Chemistry, 24 (2005) p. 199-207.

19. S. Mathison E. Bakker, Analytical Chemistry, 70 (1998) p. 303-309.

20. B. Jung, R. Bharadwaj, J.G. Santiago, Analytical Chemistry, 78 (2006) p. 2319-2327.

CHAPTER TWO

MEMS FABRICATED NANOPORES AND MICROPORES FUNCTIONALIZED WITH CHROMATE-SELECTIVE SOLVENT POLYMERIC MEMBRANE

Daniel C. Rieck[a], Bong-Jae Park[a], David F. Moffett[b], David A. Kidwell[c], Bingwen Liu[a], Gary J. Cheng[d], Bernard J. Van Wie[a,*]

[a] School of Chemical Engineering and Bioengineering, Washington State University, Pullman, WA 99164-2710, USA

[b] School of Biological Sciences, Washington State University, Pullman, WA 99164-4236, USA

[c] Naval Research Laboratory, Washington, District of Columbia 20375, USA

[d] School of Industrial engineering, Purdue University, West Lafayette, IN 47906, USA

[*] Corresponding Author. Tel: (509) 335-4103; FAX: (509) 335-4806

Keywords: Ion Selective Electrodes, Nanosensors, Microsensors, Chromate, Aliquat336, MEMS

Prepared for submission to Sensors and Actuators B: Chemical

2.2 Abstract

We developed chromate Ion Selective Electrodes (ISEs) by functionalizing nano- and micropores, fabricated using MEMS techniques, with a solvent polymeric membrane consisting of 7.7:62.2:31.1 wt % Aliquat336:2-NPOE:PVC. Using coated wire electrodes we demonstrated a response slope of −61.7 ± 2.4 mV decade^{-1}, a Limit of Detection (LOD) of $3.0\times10^{-6} \pm 1\times10^{-6}$ M, and selectivity coefficients ranging from 1.3×10^{-2} for SCN^- down to 5.0×10^{-5} for SO_3^{2-}. We achieved similar performance with our nano- and micro-scale ISEs; a nano-scale ISE 100 nm in diameter showed a response slope of −65.2 ± 4.2 mV decade^{-1} and a LOD of $1.8\times10^{-5} \pm 6\times10^{-6}$ M, versus −58.6 ± 5.6 mV decade^{-1} and $2.1\times10^{-5}\pm1.1\times10^{-5}$ M for a micro-scale ISE 30 μm in diameter. The micro-scale ISE response times averaged 40 s, while nano-scale ISE response times averaged 29 s. Electrical resistance measurements were in the GΩ range for the micro-scale ISEs and up to TΩ for the nano-scale ISEs. We used resistances to predict pore sizes, achieving agreement between actual and predicted diameters of 3% and 18% for a 100 nm nanopore and a 30 μm micropore, respectively. Atomic force microscopy (AFM) imaging of a micro-scale ISE 30 μm in diameter revealed a properly formed micropore and cast membrane, with the exposed membrane diameter exceeding that of the pore opening by 1.7 times.

2.3 Introduction

Chromium pollution from industrial waste continues to present a significant and scientifically interesting regulatory problem around the world. Kimbrough et al., discuss at length how the chemistry of chromium presents a unique regulatory challenge, particularly because of the capability of chromium(III) and chromium(VI) to interconvert readily under various conditions in the environment and as well as inside organisms [1]. Hence chromium(III), an essential trace element for human health, is dynamically connected to chromium(VI) which is quite toxic to humans and animals. Gochfeld notes how this chemistry of chromium creates problems for analysis, since interconversion can easily occur during handling, digesting, or extracting sample, such that oxidation or reduction may result [2]. Hence trace amounts of chromium are determined at present by a combination of applying standardized field sampling protocols and performing laboratory analyses using sophisticated techniques including AAS, ICP-AES, and ICP-MS [1].

The conventional analytical approaches for chromium analysis, however, require considerable expense and are time consuming, making them prohibitive for routinely analyzing large collections of samples – creating an impetus to develop alternatives. Yang et al. demonstrated how capillary electrophoresis can be used for the sensitive, selective, and simultaneous determination of chromium(III) and chromium(VI), presenting advantages of simplicity, low operating cost, and lower analysis time against other laboratory methods, but it remains a method confined to the laboratory [3]. Optical sensors that detect optical effects using adsorption, reflection, or luminescence spectrometry have also been developed and include sensors based on either the intrinsic optical properties of analytes, chromogenic and fluorogenic dyes, quenchable fluorophores, or ionophores [4-6]. They suffer, however, from several

limitations involving their selectivity, limits of detection, dynamic ranges, applicability to specific problems, and reversibility.

A variety of ionophores have been identified for use in making chromium(III) and chromium(VI) Ion Selective Electrodes (ISEs) including Aliquat336 [7]; C-thiophenecalix[4]resorcinarene [8]; tri-*o*-thymotide [9]; 18-crown-6, dibenzo-18-crown-6, and calix[6]arene [10]; bis(acetylacetnato) cadmium(II) [11]; glyoxal bis(2-hydroxyanil) [12]; 3,10-*c*-*meso*-3,5,7,7,10,12,14,14-octamethyl-1,4,8,11-tetraazacyclotetradecane diperchlorate [13]; and DABAm4 [14]. ISEs offer advantages of speed and ease of use, low cost, good selectivity, portability, fast response times, and a wide dynamic range; selectivity and detection limits, however, can be inferior to alternative techniques. Bakker and Pretsch describe how the free ion activity detected by ISEs is very different analytical information from the labile concentration which is detected by voltammetric methods, and the total concentration which is detected by atomic spectrometric methods [15]; and how ion activity information may be especially useful for speciation and bioavailability studies. Though the free ion activity measured by ISEs is often the relevant driving force behind chemical and biochemical reactions, the Limit of Detection (LOD) of ISEs has traditionally been confined to micromolar ranges and the magnitude of the free ion activity in a real sample may easily fall below this threshold.

Even if the free ion activity of an analyte remains at or above the ISE LOD, the interferents present in real world samples may still make it difficult to measure by necessitating the application of predictive models that, while reliable, require information about interferent quantities and complicate the overall analysis. These limitations mean that ISEs are barely adequate for use as sensors in the regulatory monitoring of chromium. For example the US EPA has set the Maximum Contaminant Level (MCL) for total chromium to 0.1 ppm, which is

equivalent to 1.92×10^{-6} M [16]. Though this value is technically above the LOD for a good chromium ISE, the activity, and therefore concentration, of the free ionic forms of chromium targeted by such ISEs may be considerably less than the total chromium concentration in a sample and may be easily masked by interference effects.

To meet these challenges pertaining to ISE LOD and selectivity, one can envision the use of lab-on-a-chip techniques with precise chemical analysis capabilities and pre-separation and concentration techniques such as isotachophoresis (ITP) [17-20] to extend the usefulness of ISEs. For example, a miniaturized ISE could be incorporated into micro-channels following ITP. Since micro- and nano-scale electrophoretic separation processes are possible [21], both micro- and nano-scale sensors would be useful. To help meet this need our lab recently developed a method for creating micro-scale pores in SU-8 negative photoresist [22], and a new method presented here for creating nano-scale pores in Si_3N_4 thin film. The aim of this paper is to demonstrate use of these pores as ISEs, implemented as ISE "chips" that can be mounted onto an electrochemical testing chamber, by functionalizing them with solvent polymeric membrane sensitive to chromium(VI). Of the several good formulations already reported [7-13], we chose to use the membrane formulation reported by Choi and Moon for a Supported Liquid Membrane (SLM) which targets $HCrO_4^-$. Beyond gaining the benefits associated with using an existing recipe, we felt further investigation of the Aliquat336-based membrane was warranted based on several aspects of its originally reported characteristics, such as the small number of interfering anions reported, its relatively high potentiometric selectivity coefficients, and its higher than usual lower LOD.

We show that our preparations as coated wire electrodes (CWEs) improve on the LODs and selectivities reported by Choi and Moon and require less ionophore for optimal performance;

our response slopes and linear ranges for the nano- and micro-scale ISEs compare well to the performance observed for CWEs; and our nano- and micro-scale ISEs are suitable for use with inexpensive potentiometers. The response times for micro-scale ISEs are double those observed for CWEs, but those of nano-scale ISEs are markedly longer and we provide rationale for how this may be improved in future preparations. We also describe techniques used to verify pore formation and filling and determine the morphology of membranes cast in the micropores.

2.4 Experimental

Chemicals

All reagents were of analytical reagent grade and used without further purification. We prepared all aqueous solutions using water purified to a resistance greater than 18 MΩ·cm in a Barnstead NanoPure Infinity Laboratory Water System (Dubuque, IA). We used the chemicals for preparing membrane cocktails as received, which included 1450 MW avg. polyethylene glycol (Sigma-Aldrich, St. Louis, MO), high molecular weight polyvinyl chloride (PVC) of Selectophore grade (Fluka, Buchs, Switzerland), 2-nitrophenyl octyl ether (2-NPOE) of Selectophore grade (Fluka), Aliquat336 (Sigma-Aldrich), and tetrahydrofuran (THF) of 99+% purity (Sigma-Aldrich). We used $FeCl_3$/HCl PC-Board Etching solution to make Ag/AgCl electrodes (GC Thorson, Inc., Rockford, IL). We used negative photoresist SU-8 2010 and its developer (MicroChem Corp., Newton, MA), and positive photoresist AZ5214 and its AZ400K developer (Clariant Corporation, Somerville, NJ) in microfabrication procedures.

We used n-type silicon wafers of 0.001-0.025 Ω·cm resistivity and 0.4 mm thickness from University Wafer Inc. (South Boston, MA) as a platform for nanofabrication. We printed the photomasks used for fabricating micropores on transparent plastic film obtained from University Publishing at Washington State University. We performed photolithography using

the contact method in a Model 500 mask aligner from Optical Associates, Inc. (San Jose, CA). We employed petri dishes (Becton Dickinson Labware, Franklin Lakes, NJ) as a source of plastic for making backing supports for processed SU-8 film. We made test chambers for the ISE chips out of 4.3 × 1.9 × 1.6 cm rectangular polystyrene boxes (Cargille Laboratories, Cedar Grove, NJ). Our MEMS fabrication work was finished in a WSU cleanroom.

Preparation of membranes

We prepared $HCrO_4^-$ selective membranes based on the method of Choi and Moon [7]. We prepared membrane cocktails with ionophore concentrations at 1, 2, 3, 7.8, 9, and 18 wt %, while holding the ratio of 2-NPOE to PVC fixed to 2:1, in order to assess the optimal recipe reported by Choi and Moon. A reference membrane cocktail developed at the U.S. Naval Research Laboratory (NRL) was prepared as recommended by Plesha et al. [23]. Equal volumes of 100 mg mL^{-1} PVC in THF and 200 mg mL^{-1} polyethylene glycol in THF were mixed together.

Fabrication of CWE arrays

Materials for constructing coated-wire electrode arrays included type II PVC rod of 0.5 inch diameter (McMaster-Carr, Cleveland, OH), 18 AWG copper wire (Radio Shack, Pullman, WA), 18 AWG silver wire of 99.99% purity (Prince & Izant, Cleveland, OH), super glue (Permatex, Solon, OH), and epoxy adhesive (Devcon, Riveria Beach, FL), and were used as described in Plesha, et al. [23]. To create the coated wire electrodes, we carefully pipetted 3 μL of membrane cocktail onto each polished copper wire surface so that it was coated completely but did not touch other membranes. We dried the membranes overnight under vacuum.

We integrated a reference electrode designed at the NRL into the sensor array as described by Plesha, et al. [23]. We drilled a center hole into the array and dispensed 25 μL of

reference membrane cocktail into the polished end of the center hole, which we dried overnight under vacuum. We then filled the center hole with a solution of 3M KCl(aq) and saturated AgCl (aq). Finally, we inserted a Ag/AgCl electrode into the hole and secured it in place with epoxy adhesive.

Fabrication and functionalization of nano- and micro-scale ISEs

The fabrication process for making our micropores is described in detail by Bingwen, et al. [22]. Briefly, we used spin coating to layer SU-8 2010 10 μm thick on a sacrificial layer of positive photoresist AZ521. We covered the coating with a photomask for the desired pore size and exposed it to UV light followed by SU-8 developer. We freed the SU-8 layer using AZ400K developer to etch away the sacrificial AZ5214layer, and then glued it onto a plastic chip for mounting. We functionalized the pores by pipetting a portion of 2.5 μL of membrane forming solution over the pore opening through the 3mm window of the mounting chip , on the chip-side of the film; applying only a portion of the entire 2.5 uL prevented bubbles from forming in the cast membrane. We dried the membranes overnight under vacuum.

For fabrication of the nanopores, we deposited a thin film of silicon nitride (Si_3N_4, thickness: 200 nm) on one side of the silicon wafer using Plasma-enhanced CVD. We deposited silicon dioxide on the other side of the wafer using thermal oxidation, and then spin-coated it with a photoresist layer used for patterning. We patterned a 600 μm by 600 μm window on the photoresist using UV lithography and etched the exposed silicon dioxide using RIE. We then wet etched the exposed silicon surface using KOH. Hence after the main frame of the sensor is fabricated, the photoresist and silicon dioxide layers are removed. The silicon nitride thin film acts both as an etch stopper and the impermeable membrane support for the sensor. We milled a

nanopore of 100 nm diameter in the center of this impermeable membrane using focused ion beam (FIB).

ISE testing and characterization

All tests were conducted at room temperature (≈22.7 ºC). Coated wire electrode arrays were tested in a magnetically stirred 4 mL solution volume. Nano and micro-scale ISE test cells were set up in a format identical to what Choi and Moon describe [7]. Nano- and micro-scale ISE chips were affixed to the test chamber using waterproof epoxy to ensure good electrical sealing. We inserted a Ag/AgCl electrode immersed in 4 mL of reference electrolyte, consisting of 10^{-4} M KCl combined with 10^{-4} M $K_2Cr_2O_7$, on the reference side of the test chamber. We inserted a reference electrode, consisting of a Ag/AgCl electrode immersed in 3 M KCl(aq) saturated with AgCl(aq) and separated from sample by a NRL reference membrane, into the sample side of the test chamber. Nano- and micro-scale ISEs were tested such that the sample side of the testing chamber was magnetically stirred.

We calibrated all sensors with an inexpensive potentiometer which was designed at the NRL, has a 10 TΩ internal resistance, and is described more fully in Plesha, et al. [23]. Linearity and limit of detection (LOD) studies were performed using the standard addition method over concentrations ranging from 10^{-8} M to 1^{-1} M. Electrode response slopes were determined by assuming an activity coefficient of unity for calibration species and fitting the modified Nicolsky-Eisenman model using nonlinear regression to calibration data [23]. The model used was:

$$E = E_0 + S \cdot log_{10}(a + U), \quad (1)$$

where E is membrane voltage, E_0 is the cell constant, S is the ISE slope, a is the activity of the analyte, and U is the coefficient of unmodeled interferents [23-26]. The advantages of this

approach are that nonlinear regression produces standard errors for parameters which can give an idea of the reliability of the calibration curve, and including the detection limit parameter U forces slopes and LODs to reflect the low concentration non-linear region of the curve.

Lower LODs were taken as the activity of $HCrO_4^-$ at the point of intersection between the linear region of the calibration curve and the final low concentration level, which is the method recommended by the IUPAC [27]. Interferences were determined using the Separate Solution Method (SSM) at matched activities [28]; we determined selectivity coefficients for SO_4^-, CH_3COO^-, Cl^-, and F^- at an ion activity of 1.16×10^{-2} M, and selectivity coefficients for SO_3^-, I^-, NO_3^-, $H_2PO_4^-$, and SCN^- at an ion activity of 0.1 M. We did not prepare calibration solutions for interfering ions in buffer. Response times were determined as the time to 90% of the steady-state EMF.

Approximate electrical resistances of nano- and micro-scale ISEs were determined using an Axopatch 200 (Molecular Devices, Sunnyvale, CA) operating with a CV-201 headstage in whole cell recording mode. Output from the Axopatch was passed through a 60 Hz noise filter and recorded to computer using a RadioShack Digital Multimeter model 22-812 (RadioShack Corporation, Fort Worth, TX). Silver/silver chloride electrodes were immersed in test electrolyte on either side of the sensor; one electrode was connected to the positive terminal of the headstage, and the other was connected to its negative terminal. We recorded the cell current as we varied the holding potential of the cell. We used the RadioShack Digital Multimeter in resistance testing mode to obtain an order of magnitude estimate of the electrical resistances of the coated wire electrode arrays.

Imaging of nano and micro-scale ISEs using atomic force microscopy

We employed atomic force microscopy (AFM) to obtain topographic images of nano- and micro-scale ISEs by using a PicoForce™ Scanning Probe Microscope equipped with a 259PF scanner (Veeco Inc., Santa Barbara, CA). Contact mode in air at room temperature was used as the scanning mode to take the AFM images over different areas of each sample using ultrasharp silicon cantilevers (spring constant: 7.5 N m−1) (MikroMasch, Portland, OR). We fixed nano- and micro-scale ISEs to a magnetic holder using double sided adhesive tape. We set the scanning area to 60 μm × 60 μm and kept the scan rate set to 1 Hz with a resolution of 256 samples per line. The AFM images we present in this study did not undergo any specific image processing except flattening, unless otherwise indicated. To determine more exact dimensions of sensor membranes, we selected line profiles to traverse the AFM images we collected.

2.5 Results and Discussion

Our rationale for producing micro and nano-scale ISE based on MEMS fabrication techniques such as UV lithography and FIB is when a membrane forming solution is applied to one side of an impermeable surface over a nano- or micro-scale pore in that surface, it will fill the hole and dry. This will expose a solvent polymeric membrane, about the diameter of the pore, on the opposing surface which will function as an ISE membrane when introduced to sample. It will perform identically to a macroscopic ISE if the experimental electrochemical cell is properly configured since the phase boundary potential of ISEs is independent of the cross sectional area of the exposed membrane surface [29]. The resistance imposed by the membrane will increase as the pore is made smaller, but will remain within the limits required by our intended use. Sensors performing according to these expectations will be compatible with lab-on-a-chip preseparation and preconcentration technology and therefore usable in-situ as a means

to interrogate micro-scale sample separation bands for trace-level analysis of chromium. Our experimental results presented here test our rationale and demonstrate the efficacy of the sensor fabrication technique.

Basic ISE membrane properties for CWE

We tested additional membrane formulations to determine the effect of lowering the ionophore concentrations below 4.6 wt %, which is the lowest value tested by Choi and Moon. Table 2.1 summarizes the slopes and LODs obtained for the various membrane formulations we tried, compared to the results of Choi and Moon. The formulations we prepared achieved LODs in the range 1.78×10^{-6} M through 5.71×10^{-6} M, which in the best case is nearly an order of magnitude lower than the lowest LOD reported by Choi and Moon. Near-Nernstian slopes of -49.5 ± 1.3 mV decade^{-1} and above were obtained for all formulations, suggesting that a lower

TABLE 2.1
Response slopes and detection limits obtained for the various membrane forming solutions, compared to the results reported by Choi and Moon (2005) [7].

Membrane Composition Aliquat336 : o-NPOE : PVC (in % w/w)	Source	Slope (mV decade^{-1})	LOD (mol L^{-1})
1.0:66.0:33.0	WSU	-50.7 ± 5.8	4.34×10^{-6}
2.0:66.7:31.3		-49.5 ± 1.3	3.65×10^{-6}
3.0:65.4:31.6		-53.0 ± 1.0	1.78×10^{-6}
7.8:62.2:30.0		-61.7 ± 2.4	3.02×10^{-6}
9.0:60.7:30.3		-52.2 ± 0.7	5.71×10^{-6}
18.0:54.8:27.2		-50.1 ± 2.9	2.34×10^{-6}
4.6:64.4:31.0 [a]	Choi and Moon	−95.5	1.09×10^{-5} [b]
8.8:61.6:29.6		−57.6 [c]	3.85×10^{-5} [c]
10.1:56.2:33.8		−61.2	2.70×10^{-5}
12.7:59.0:28.3		−57.3	1.55×10^{-5}
12.8:44.5:42.8		−60.2	2.70×10^{-5}
17.4:24.3:58.3		−74.6	3.37×10^{-5}
18.2:55.2:26.6		−62.9	2.45×10^{-5}
23.0:0.0:77.0		–	–

[a]Choi and Moon reported their membrane composition data in mL Aliquat 336 : mL 2-NPOE : gm PVC. We converted these values to weight percents, using density values at 25 ºC for Aliquat336 of 0.884 gm mL^{-1} and for 2-NPOE of 1.04 gm mL^{-1}.
[b]Choi and Moon reported limits of detection in ppm Cr(VI), and we converted these values into mol L^{-1} by assuming a water density of 0.9970 gm mL^{-1} (true at 25 ºC). They did not report errors.
[c]Choi and Moon provided original calibration data points for this membrane composition. We used nonlinear regression to fit the extended Nicolsky-Eisenman model to their data as described in the manuscript. The model parameters and their standard error are reported in the table, versus the original values reported by Choi and Moon of −53.7 mV/decade for the slope and 2.01×10^{-5} mol L^{-1} for the LOD.

concentration of ionophore can produce excellent ISE performance. Fig. 2.1 shows the results of the calibration experiment for our optimally performing CWE membrane, which was 7.8:62.2:30.0 wt % Aliquat336:2-NPOE:PVC, compared to Choi and Moon's optimally performing SLM,

which was 8.8:61.6:29.6 wt %. This CWE membrane achieved a Nernstian slope of −61.7 mV decade^{-1}, which is higher than that of Choi and Moon's SLM by 7.1%; and an LOD of 3×10^{-6} mol L^{-1}, which is over an order of magnitude lower than the result obtained by Choi and Moon. These results suggest the CWE produces a superior ISE response compared to the SLM. When we used calibration solutions prepared in 0.1 M acetate buffer vs. 0.01 M, we obtained a near Nernstian slope lower than Choi and Moon's result and differing by 7.5%, but a LOD reduced by almost an order of magnitude. This result indicates that using acetate buffer of 0.01 M concentration or lower provides excellent control of sample pH without significantly interfering with ISE

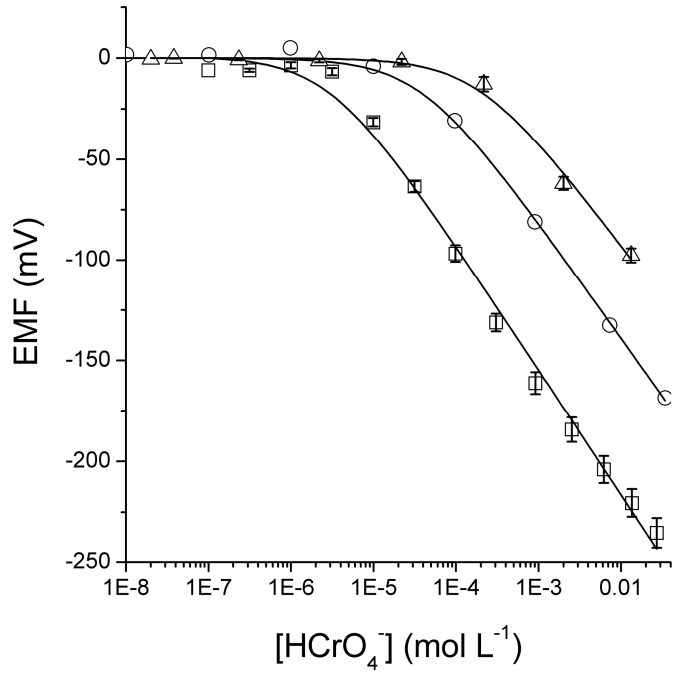

Fig. 2.1. Potentiometric calibration curves of our coated wire electrode using calibration solutions in 0.01 M acetate buffer (□) and 0.1 M acetate buffer (△), compared to Choi and Moon's supported liquid membrane (○) [7]. A membrane recipe consisting of 7.8:62.2:30.0% (w/w) Aliquat336:2-NPOE:PVC was used for both coated wire electrodes, which was of similar composition to Choi and Moon's membrane of 8.8:61.6:29.6% (w/w) Aliquat336:2-NPOE:PVC. Data points for all calibration curve graphs are average values (n = 3). The LODs by the recommended IUPAC method were: 3.03×10^{-6} M (□), 1.46×10^{-4} M (△), and 3.55×10^{-5} M (○). The calibration curves shown are the result of a fit of the extended Nicolsky-Eisenman model to each set of data using nonlinear regression. Values and standard errors for the slope parameter S, in units of mV $\log_{10}{}^{-1}$(a), were: −61.7 ± 2.4 (□), −53.3 ± 3.8 (△), and −57.6 ± 2.6 (○); for the cell constant parameter E_0, in units of mV, were: −334.1 ± 7.6 (□), −201.7 ± 9.0 (△), and −248.0 ± 6.6 (○); for the detection limit parameter U, in units of mol L^{-1}, were: $3.02\times10^{-6} \pm 1.04\times10^{-6}$ (□), $1.66\times10^{-4} \pm 4.50\times10^{-5}$ (△), and $3.85\times10^{-5} \pm 9.57\times10^{-6}$ (○).

operation.

Conventional wisdom concerning solvent polymeric membranes dictates that typically an ionophore concentration of about 1% (w/w) is sufficient, and that the ratio of plasticizer to PVC should be 2:1 by weight [30]. This is reflected in a majority of the solvent polymeric membrane recipes employing different ionophores and targeting chromium ions (including Cr^{3+}, $HCrO_4^-$, and CrO_4^{2-}) [8-10, 12], though that of Aradkani, et al. [11] and Singh, et al. [13] are exceptions. The micromolar LODs obtained for all membrane formulations displayed in Table 2.1 are more in line with the traditional LOD for an ISE [15] and show that the CWE membrane has a superior sensitivity compared to the SLM of Choi and Moon by one to two orders of magnitude. All electrodes gave response times comparable to what is displayed for the 7.8 wt % ionophore in section 2.5. Ultimately we found no significant performance difference resulted from using more than 1% (w/w) ionophore. This demonstrates that effective Aliquat336-based solvent polymeric membranes can be prepared with much lower ionophore compositions than originally reported.

The improvement of the LOD when our CWE calibration data is compared to that of Choi and Moon is difficult to explain. Some factors affecting attempts to reproduce LOD data for an ISE are discussed by Buck and Linder [27], and include sample composition, history and precondition of the electrode, stirring rate; and details of the measured data, such as the number of measurements taken and the standard deviation of each calibration data point. As the LODs differ by one to two orders of magnitude, it is problematical to argue that the discrepancy is due to these aspects. However, a strong explanation comes from the different implementations of the electrodes. Choi and Moon used an inner filling electrolyte containing 10^{-4} M $K_2Cr_2O_7$ at an unspecified pH on the reference side of their SLM, whereas an inner filling electrolyte is avoided

in a CWE. Using the SLMs in the pH range of 3.5-6 which they indicated would result in $HCrO_4^-$ dominating the aqueous chromium (VI) equilibrium at possible mol % values from 98.8 to 75.3, respectively [31]. This places $HCrO_4^-$ in contact with the ISE membrane, and when the membrane is exposed to dilute sample, the theoretical work of Bakker and Mathison [32] demonstrates $HCrO_4^-$ will be coextracted with cations into the membrane. This results in a $HCrO_4^-$ concentration gradient counterbalanced by complexed ionophore and leading to a net flux of electrolyte across the membrane and into membrane-sample interface, perturbing its composition by raising its $HCrO_4^-$ level. Since the interfacial composition dictates the LOD [33], the contributions of more dilute test solutions on the sample side of the membrane will be masked, effectively limiting the observable LOD based on the $HCrO_4^-$ concentration of the inner filling electrolyte. This effect is reported to occur even at relatively dilute concentrations of inner filling electrolyte [33].

The fact that the membrane formulation lacks added lipophilic cationic sites and has a relatively high concentration of ionophore would tend to worsen this problem. Lipophilic cationic sites tend to limit cation extraction, which also limits coextraction of the measured anion and hence its flux into the membrane-sample interface. The high concentration of ionophore in the membrane formulation allows more $HCrO_4^-$ to be extracted from the inner filling solution and complexed, leading to a higher concentration gradient across the membrane. Bakker and Mathison's estimate of the upper limit for the lower LOD [32] predicts a value of 5×10^{-5} M for the membrane recipe in question, which is in the range of the Choi and Moon's reported LOD; but their estimate is based on an ionophore concentration of 1 wt %, so the upper limit for the Aliquat336 membrane could be ~20 times higher based on its concentration and higher molecular weight. Hence it is unlikely that a concentration of 10^{-4} M analyte will lead to the

complete saturation of ionophore to which this value applies, so a more concentrated reference electrolyte could lead to a more severe effect on the LOD. We explore this problem further when discussing our micro-scale ISE results (see section 2.5).

We used buffering in the calibration experiments for linearity and LOD studies to control the pH of the calibration solutions. Based on the work of Tandon, et al., for total chromium concentrations of up to 10^{-3} mol L^{-1} the pH range must be kept within 2.39-4.85 in order to maintain at least 90 mol-% of $HCrO_4^-$ [31] (these figures are based on a value of 33.3 for the equilibrium constant associated with the equilibrium between $HCrO_4^-$ and $Cr_2O_7^{2}$ [31]). For example, when we prepared the calibration solutions in nanopure water the pH ranged from 4.2 to 6.5 and averaged 5.3 ± 0.7. In contrast, when prepared in water buffered at pH 3.9 using a 0.01 M acetate system, the pH ranged from 3.6 to 4.0 and averaged 3.8 ± 0.1. This demonstrates buffering is necessary to maintain $HCrO_4^-$ as the dominant form of chromium (VI), or it could easily fall as low as 50 mol-% which occurred in one instance for calibration solutions from 10^{-8} to 10^{-3} M as the pH was consistently above 5. The use of buffer introduces the concern that it may affect ISE response. This is reflected by the order of magnitude increase in LOD evident when comparing calibration curves from solutions calibrated in 0.01 M acetate buffer to those calibrated in 0.1 M buffer, which is due both to interference from the acetate ion and the effect of increased ionic strength. Hence the conjugate base present in buffer formulations must be tested to rule out these effects. We also found it critical to test the pH of calibration solutions in general, because the $HCrO_4^-$ mol-% rapidly falls below 90% when the total chromate concentration increases beyond 10^{-3} M.

Potentiometric selectivity coefficients for CWE membrane

We determined the interferences of common ions for the membrane in order to compare with the results of Choi and Moon and to obtain selectivity coefficients for ions of interest that they did not test. We used the SSM at identical activities to determine selectivity coefficients[28] which was one of the methods used in Choi and Moon's work, the other being the Fixed Interferent Method (FIM). We did not perform the FIM because the SSM is simpler; furthermore, though the FIM is considered to be more accurate, the SSM method is deemed an acceptable alternative [27]. Our experimentally determined selectivity coefficients are summarized in Table 2.2, and Figure 2.2 displays the EMF data for each solution used in the SSM and containing either the primary ion or a single interferent. For the Cl^- ion we achieved results similar to those of Choi and Moon when considering data obtained using $HCrO_4^-$ calibration solutions prepared in 0.1 M acetate buffer. For the other the other ions studied by Choi and Moon, namely SCN^-, I^-, NO_3^-, SO_4^-, our values are approximately an order of magnitude better even when using the calibration for $HCrO_4^-$ in 0.1 M acetate buffer and one to three orders of magnitude better when

TABLE 2.2
Selectivity coefficient values obtained by the Separate Solution Method.

Interfering Ion	$Log_{10}(K_{A,B})$	
	Against $HCrO_4^-$ Calibration in 0.01 M Buffer[a]	Choi and Moon (no buffering) [c]
SCN^-	−1.9 ±0.4	1.14 (0.69, FIM)
I^-	−2.8 ±0.4	0.049 (−0.43, FIM)
NO_3^-	−3.2 ±0.4	−0.54
$H_2PO_4^-$	−3.4 ±0.6	−
F^-	−3.4 ±0.5	−
Cl^-	−3.5 ±0.4	−1.68
CH_3COO^-	−3.5 ±0.5	−
SO_4^{2-}	−4.0 ±0.5	−3.00
SO_3^{2-}	−4.3 ±0.5	−

[a]The selectivity coefficients in this column were calculated using a primary ion calibration curve obtained from calibrating a coated wire electrode in 0.01 M Acetate/Acetic Acid buffering system at a pH of 3.9. Error was determined from the standard errors of the parameter values resulting from nonlinear curve fitting.
[b]Choi and Moon [7] indicate their primary ion calibration solutions were prepared in deionized water at pH ranging from 3.5-6.0. They did, however, use an inner filling electrolyte containing 10^{-4} M $K_2Cr_2O_7$, whereas coated wire electrodes avoid inner filling electrolytes altogether.

using the calibration for $HCrO_4^-$ in 0.01 M acetate buffer. For SCN^-, we showed that the membrane responds significantly better to $HCrO_4^-$, whereas for Choi and Moon the membrane actually responded better to SCN^- than $HCrO_4^-$. Though our selectivity coefficients are lower than that of Choi and Moon, we also determined that the Aliquat336 based membrane had a higher Cr(VI) selectivity against divalent interfering ions than against monovalent interfering ions, as the interference effects are in the order $SCN^- > I^- > NO_3^- > H_2PO4^- > F^- > Cl^- > CH3COO^- > SO_4^{2-} > SO_3^{2-}$. The higher selectivity coefficients obtained by Choi and Moon can be explained by the combination of the membrane formulation and their use of inner filling electrolyte containing significant $HCrO_4^-$ from 10^{-4} M $K_2Cr_2O_7$ at unspecified pH, as for both the Fixed Interference Method (FIM) and SSM the true LOD of the electrode will be obscured by the flux of $HCrO_4^-$ from inner filling electrolyte into the membrane-sample interface. And as established by Pretsch, et al. [33], the LOD of an ISE greatly affects its potentiometric selectivity coefficients.

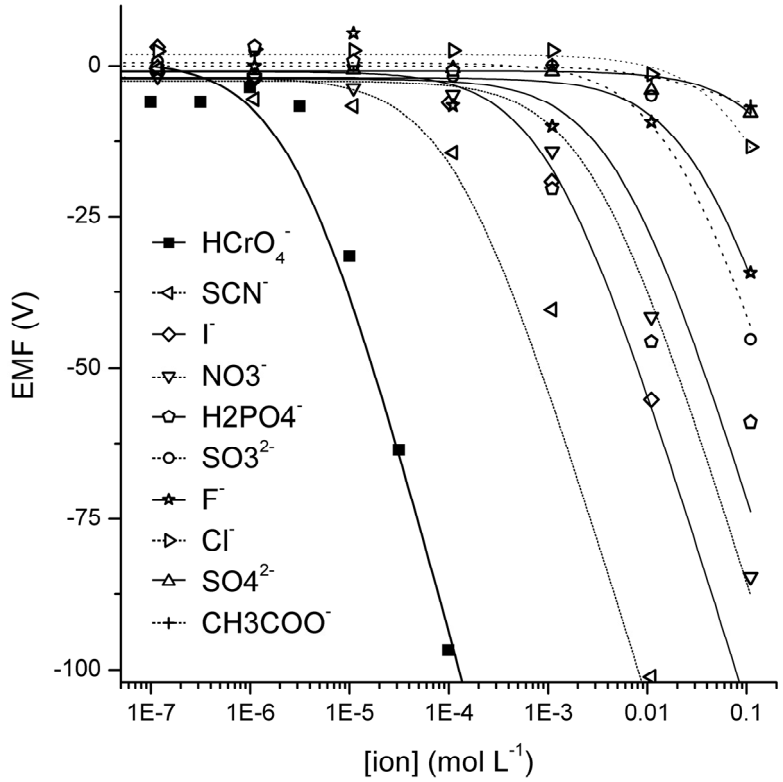

Fig. 2.2. Potentiometric calibration curves used in the SSM to determine selectivity coefficients for common interfering anions. The calibrations appearing in this graph for interferents were obtained using a coated wire electrode exhibiting a slope of -61.7 mV/decade and an LOD of 3×10^{-6} M, when calibrated with $K_2Cr_2O_7$(aq) solutions buffered using a 0.01 M Acetate/Acetic Acid system. Error from nonlinear regression is reflected in the calculation of selectivity coefficient values based on these curves and is indicated in Table 2.2.

Another explanation that may arise for the lower LOD of the CWE demonstrated in the previous section is the relatively high selectivity coefficient reported by Choi and Moon for bicarbonate ion with a value of 0.38 by the Fixed Interference Method (FIM) and 0.41 by the

Separate Solution Method (SSM) [7]. Though bicarbonate ions can be quickly introduced into purified water from equilibria involving dissolved carbon dioxide and carbonic acid, it is doubtful that this accounts for the discrepancy. The bicarbonate ion concentration would have to be 1.01×10^{-4} M to account for the full effect, based on a selectivity coefficient of 0.38 for HCO_3^-; even when considering the upper level of 2500 ppm for the range of typical indoor atmospheric CO_2 concentrations [34], the bicarbonate ion and dissolved CO_2 concentrations still only reach 6.01×10^{-6} M and 8.40×10^{-5} M, respectively, based on carbonic acid equilibrium constants taken at 25 ºC. This implies that it is not possible for enough bicarbonate ions to be present in calibration solutions to account for the LOD.

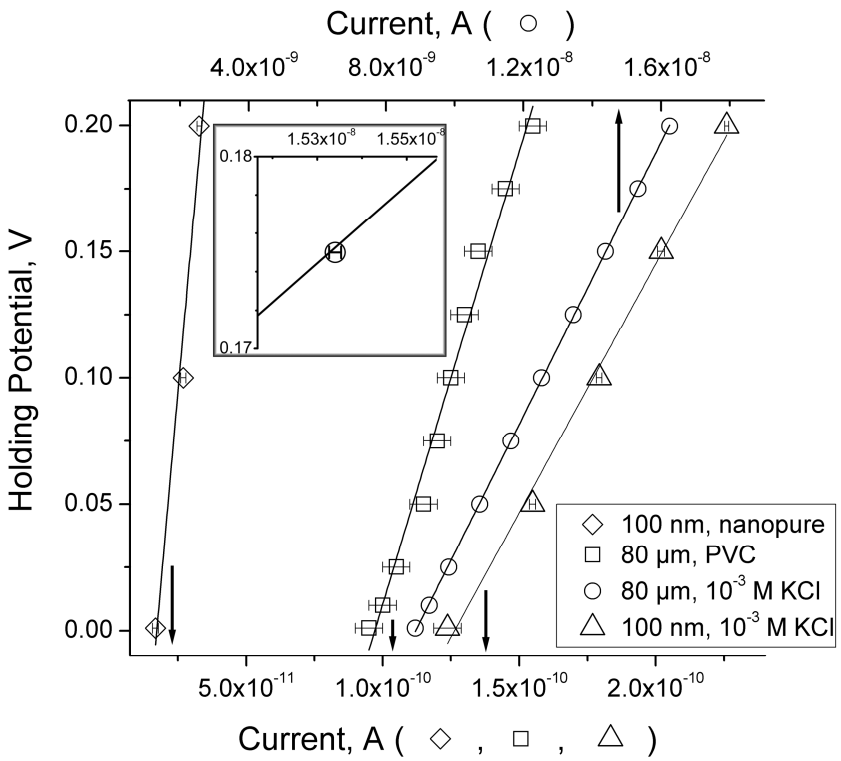

Fig. 2.3. A graph of current readings at various holding potentials for an 80 µm micropore without membrane (○) and tested in nanopure water, the same micropore functionalized with 7.8:62.2:30.0% (w/w) Aliquat336:2-NPOE:PVC membrane (□) and tested in nanopure water, and a 100 nm nanopore (△) tested in 10^{-3} M KCl (aq), and the same nanopore functionalized (◇) and tested in nanopure water. Though current is the dependent variable, it is plotted on the x-axis because the slope of a linear plot of voltage versus current is equivalent to the circuit resistance according to Ohm's law. Current values exhibited measurement errors of ±0.01 nA (○) and ± 0.005 nA (□, △, ◇) and are reflected in the error bars (for ○ the error is shown in the inset).

Electrical resistance of sensors

The electrical resistance of our pores with and without membrane is a very useful measurement, as it can allow us to predict pore size, tell us if a pore is functionalized, and indicate what quality of potentiometer is required by the sensors. Figure 2.3 shows electrical data collected with an

Axopatch 200, while testing an 80 μm micropore, with and without a membrane and using nanopure water as the test electrolyte, and a nanopore using 10^{-3} M KCl(aq) as the test electrolyte. Axopatch patch clamping devices are known for their high internal resistances, and they have been used to take electrical measurements on systems imposing a load of up to 50 GΩ [35]. Hence we used them to obtain current measurements as holding potentials are varied. Figure 2.3 shows a linear relationship between holding potential and current, reflecting ohmic behavior. This enables us to calculate the resistances from the linear slopes, since the electrical resistance of the pore should dominate the test cell.

The resistances calculated from such relationships for various pore configurations are summarized in Table 2.3. The resistance measurements indicated for the coated wire electrode arrays give an order of magnitude estimate, due to the inaccuracies inherent in using a digital multimeter to estimate resistance (such as electrode polarization). However, the resistances imposed by the CWEs were so small that the 19.56 nA current upper limit for the Axopatch headstage was exceeded regardless of holding potential. The Axopatch was unable to report current measurements for micropores immersed in 10^{-3} M KCl for the same reason, so we used the digital multimeter to measure it instead and

TABLE 2.3
Electrical resistance of different sensor configurations

Sensor description[a]	Resistances, GΩ	
	Conducting Medium	
	Nanopure H_2O	1×10^{-3} M KCl (aq)
Coated wire sensor array	0.0043 ± 0.0018	0.0043 ± 0.0028
Micropore (80 μm)	0.0271 ± 0.0001	0.0017 ± 0.0005[b]
Nanopore (100 nm)	12.1 ± 1.9	2.0 ± 0.1
Functionalized Micropore	3.6 ± 0.2	4.3 ± 0.7
Functionalized Nanopore	40.2 ± 5.4	34.9 ± 6.4

These resistance values were determined using our Axopatch 200 with a CV-201 headstage, except the resistances for the coated wire sensor array which were estimated using the RadioShack Digital Multimeter 22-812.
[a] Sensors described as micropores and nanopores were not functionalized with solvent polymeric membrane, whereas sensors described as functionalized nano- and micropores were functionalized with 7.8: 62.2: 30.0% (w/w) Aliquat336:2-NPOE:PVC solvent polymeric membrane.
[b] When the micropore was immersed in 1×10^{-3} M KCl (aq), an invariant 19.56 nA resulted throughout the range of possible holding potentials. Hence the resistance was measured with the digital multimeter.

obtained a relatively low value of 1.7 MΩ. We note that the resistances for the functionalized nanopores seem too low based on the resistance change associated with changing the conducting medium inside the micropores from 10^{-3} M KCl to solvent polymeric membrane. The currents associated with functionalized nanopores were so low, however, that the associated resistance values are based on currents measured after a jump from a 1.0 mV holding potential to 199.8 mV and are plagued by high noise. Hence it is likely that the true resistance values for the functionalized nanopores are much higher.

The resistances of pores quantitatively reflect their predicted geometry. We can approximate the pore as a perfect cylinder and model its electrical resistance as

$$R_{sensor} = \frac{\rho \times L}{\pi \times r^2} + \frac{\rho}{4 \times r}, \quad (2)$$

where ρ is the resistivity of the conducting medium inside the pore, L is its depth, and r its radius. The first term of eq. 2 refers to the electrical resistance imposed by the medium filling the pore. The second term is from the Hall model [36] and is used to model the access resistance, which must be accounted for in small pores. It arises as current paths from bulk electrolyte converge into the pore, and is most significant when pore geometry is relatively wide and short [37]. Using this model, we calculate the diameter of the nanopore based on its measured resistance, the resistivity for 10^{-3} M KCl electrolyte of 6.81 kΩ·cm [38], and an approximate pore depth of 0.2 μm, obtaining a value of 103 nm. This is only 3% different from the approximate pore diameter of 100 nm predicted from the pattern size of the nanofabrication protocol, confirming the existence of a properly formed nanopore.

Considering the micropore is more difficult due to CO_2 uptake by our nanopure water. To illustrate, from a micropore depth of 10×10^{-6} μm, a diameter of 80 μm, and nanopure water

resistivity of 18.2 MΩ·cm, we calculate a resistance of 1.50 GΩ, yet we obtained only 27.1 MΩ. If, however, we assume the water is in equilibrium with the ambient atmosphere and dissolved carbon dioxide is the only source of ionic impurities, then the bicarbonate equilibria would result in a reduced resistivity of 0.4 MΩ·cm, based on a measured pH of 5.2 and a molar conductivity of 0.0394 m^2 S mol^{-1} due to hydronium and bicarbonate ions [39]. Using this value we predict a micropore diameter of 94.2 μm using the resistance model, which is also only 18% different from the approximate pore diameter of 80 μm predicted from the pattern size of the microfabrication protocol, providing good evidence of a properly formed micropore. This analysis can also be performed for the nanopore immersed in nanopure water, and yields only a 1% difference between the predicted and actual pore diameters.

The data in Table 2.3 properly reflect pore functionalization. We used the resistance model to estimate the resistivity of the solvent polymeric membrane used to functionalize pores. We calculated values of 43.7 MΩ·cm and 52.2 MΩ·cm based on the resistance of the 80 μm micro-scale ISE when immersed in nanopure water and when immersed in 0.001 M KCl electrolyte, respectively. Though we did not have resistivity data on this membrane formulation, these values are consistent with literature. For example, PVC plasticized with 66 wt-% di-2-ethylhexyl phthalate can have a resistivity as low as 1.63 MΩ·cm [40], but higher values in the range of our value are possible depending on the type of plasticizer and the membrane composition [30]. Though the values for the functionalized nanopore resistances are suspect for reasons indicated previously, they reflect a conducting medium resistivity that is higher than the nanopure water. Hence though they do not quantitatively reflect the PVC resistivity, they correctly exhibit the trend that it exceeds that of the nanopure water.

Finally, the resistance data give us an idea of what kind of potentiometer is needed to take measurements with the sensors. A potentiometer must have an internal resistance greatly exceeding the load of the sensors; otherwise it will draw too much current and skew the measurement. The micro-scale ISE's resistances of 3.6 GΩ - 4.3 GΩ are less than 10 GΩ, implying that a 10 TΩ internal resistance is more than adequate for working with them. Though the measured electrical resistance of the functionalized nanopore was only around 35-40 GΩ, the resistance model predicts it could be as high as 14.6 TΩ based on the nanopore's geometry and the average value of the solvent polymeric membrane resistivity calculated from the data for the functionalized micropores.

Nano- and micro-scale ISE morphology

It is important to know the morphology of ISE membranes produced using our methods, since we apply membrane forming solution to our pores with a pipette. Ultimately, we want to create micro- or nano-sized ISE membranes while using macroscale fabrication techniques, e.g. pipetting of membrane forming solution into the vicinity of the pore region. This is important when considering potential applications for such small ISEs. One example is the interrogation of a 200 μm sample band formed during isoelectric focusing; if we are to sense concentration accurately as the band flows past an ISE, the ISE itself must be smaller than the band.

We hypothesized that solution would fill the pore and even pool out slightly on the opposing side, implying that the membrane surface area exposed to solution would exceed the pore surface area. To test this we imaged micro-scale ISEs using AFM, which is an excellent imaging tool and does not require sample preparation and even preserves the sample from disruption while surface character is being measured. Figure 2.4 shows a topology image of an

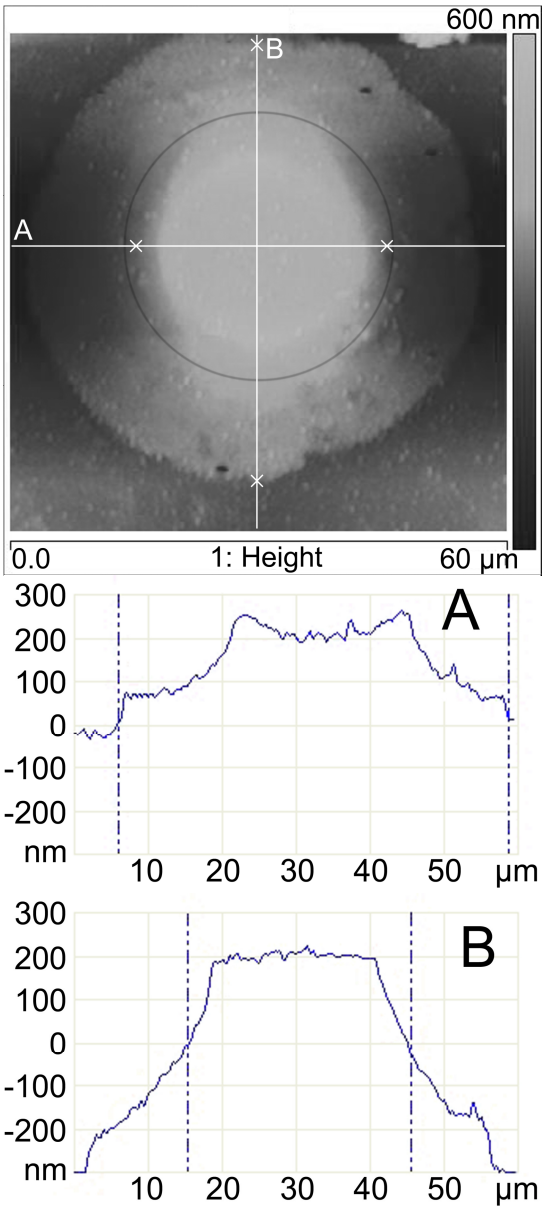

Fig. 2.4. Topology image and line profiles obtained by AFM, showing a micro-scale ISE membrane which was cast by applying roughly half of the contents of a pipette tip containing 2.5 µL of 7.8:62.2:30.0% (w/w) Aliquat336:2-NPOE:PVC membrane forming solution to a micropore of 30 µm diameter in SU-8. Only a portion of the pipette contents is expelled to avoid the presence of air bubbles in the dispensed membrane forming solution. The faint dark ring centered inside in the membrane was digitally added to indicate a rough outline of the micropore, which is based on the size of the pattern used to etch it. The membrane is approximately 50 µm in diameter, which is 1.7 times larger than the diameter of the micropore. The white lines were digitally added along with X's and correspond to the horizontal line scan profile (A) and the vertical line scam profile (B).

ISE membrane cast onto a 30 µm pore with two AFM profile scans taken perpendicular to each other. The X's on the AFM image correspond to the vertical dashed lines plotted on the profile scan images. The figure shows by way of a dark circle that was added digitally a diameter of 30 µm that corresponds to the size of the photomask used to etch the pore. We centered this dark circle about the bump in the center of the membrane, as this bump corresponds to the location of the actual pore since its height reflects the location that the membrane forming solution flowed through from the opposite side. The results clearly show evidence of a properly formed membrane that is 50 µm in diameter or 1.7 times larger than the pore on which it was cast, demonstrating that pore size does not exactly correspond to final membrane size. Because the membrane is not much larger than the pore our hypothesis that a macroscale application of membrane forming solution results in a micro-sized ISE is proven.

According to Figs. 2.4A and B the

approximate height of the membrane directly over the central 30 μm diameter pore is 200 nm while the extreme outer edge of the membrane protrudes above the surface by a mere 100 nm. Scan Profile B shows a slightly concave surface that is 50 nm higher than its outer edges. Based on these measurements, less than a nanoliter of membrane protrudes out of the pore face. The height and amount of solvent polymeric membrane are expected to have little consequence in terms of perturbing any separation bands that may pass over an ISE embedded in the wall of a channel that is on the order of 10 μm wide, though when channels are on the submicron scale the perturbation of passing fluid is expected to become more important.

In an attempt to image the nano-scale ISEs using AFM, we could not distinguish the membrane from the other surface features and dust particles on the silicon surface (data not shown). Compounding the problem is the inability to determine the approximate position of the pore given the fabrication technique; there was not a set of crosshairs built into the mask we used. However, as stated earlier resistance data collected on the nano-scale ISEs indicate the pore is on the order of 100 nm in diameter and is therefore suitable for use in channels on the nano-scale dimension or for analyzing ISE bands that are submicron in length.

Nano- and micro-scale ISE performance compared to CWEs

Figure 2.5 shows the calibration curves of a nano-scale ISE formed from a nanopore 100 nm in diameter and a micro-scale ISE formed from a micropore 30 μm in diameter compared to a CWE. All three electrode configurations showed similar performance characteristics, albeit with slight differences. For example, both the nano- and micro-scale ISEs give similar LODs in with values of 1.8×10^{-5} M and 2.1×10^{-5} M, respectively, which is nearly an order of magnitude higher than the 3.0×10^{-6} M LOD of the CWE. These LOD values are nearly identical to what

Choi and Moon obtained, which is consistent with the fact that the same experimental setup was used for the nano- and micro-scale ISEs, and that they essentially constitute miniaturized SLMs.

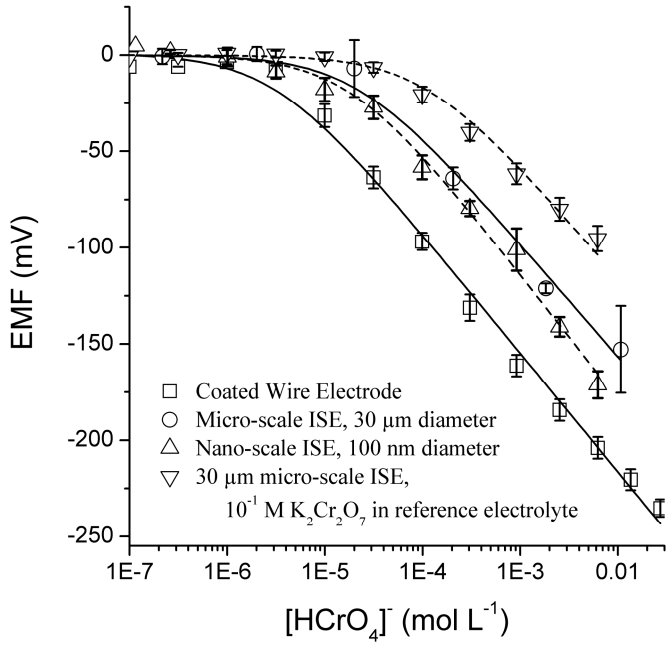

Fig. 2.5. Potentiometric calibration curves of a micro-scale ISE formed from a 30 µm micropore (○) and a nano-scale ISE formed from a 100 nm nanopore (△), compared to a CWE (□), and all with identical membrane compositions of 7.8:62.2:30.0% (w/w) Aliquat336:2-NPOE:PVC. The micro-scale ISE was also calibrated when using a reference electrolyte having its $K_2Cr_2O_7$ concentration increased to 0.1 M (▽). The figure confirms all three electrodes behave similarly with LODs on the order of 10^{-5} M or better and a Nernstian response slope of -61.7 ± 2.4 mV decade^{-1} (□) for the CWE, -58.6 ± 5.6 (○) for the micro-scale ISE and a slightly super-Nernstian value of -65.2 ± 4.2 (△) for the nano-scale ISE. Values and standard errors for the cell constant parameter E_0, in units of mV, were: -269.6 ± 16.2 (○) and -314.1 ± 12.8 (△). Values and standard errors for the detection limit parameter U, in units of mol L^{-1}, were: $2.09\times10^{-5} \pm 1.82\times10^{-5}$ (○) and $1.79\times10^{-5} \pm 5.7\times10^{-6}$ (△). The more concentrated reference electrolyte resulted in an increase of the LOD to 8.1×10^{-5} M.

Compared to the -61.7 ± 2.4 mV decade^{-1} Nernstian response slope of the CWE, that of the micro-scale ISE is only 5% lower at a value of -58.6 ± 5.6 mV decade^{-1}, and the slightly super-Nernstian response slope of the nano-scale ISE is only 5.7% greater at a value of -65.2 ± 5.6 mV decade^{-1}. Using a reference electrolyte containing 0.1 M $K_2Cr_2O_7$ to calibrate the micro-scale ISE (versus the normal 10^{-4} M $K_2Cr_2O_7$) resulted in an LOD of 8.1×10^{-5} M, which is over a half-decade increase in the LOD. This confirms that introducing $K_2Cr_2O_7$ into the reference electrolyte can affect the LOD of the SLM. Interestingly, lowering the concentration of $K_2Cr_2O_7$ in the reference electrolyte to 10^{-7} M did not appreciably affect the LOD, implying that the difference in LOD between the CWE and SLM may be due to the elimination of the inner electrolyte in the CWE.

Data in Figure 2.6 reveal the fastest response times for the different electrodes in our study, where response times are defined as the time taken for an ISE to achieve an EMF that is

90% of its steady state value after adding an aliquot of a solution containing a higher concentration of analyte and are calculated as the average values (n=6) for $10^{-5.5}$ to 10^{-1} M additions for the data presented in Fig. 2.5. The average response times for the CWE, nano-scale ISE, and micro-scale ISE were 23.5 ± 12.5 s, 28.8 ± 6.1 s, and 40.2 ± 25.4 s, respectively. The CWE has a response time in the typical range of 20 seconds or less observed for chromium ISEs in the literature [8-13]. The response time for the nano-scale ISE was only 22.7% greater than this value, an excellent result given the error of the measurement. The micro-scale ISE response time was 71.1% greater that of the CWE, but had a much higher measurement error. We attributed this to the fact that calibration standards were continuously added for the micro-scale ISE, creating significant measurement noise and making it more difficult to determine the response time accurately; Fig. 2.6 shows that all three electrode configurations are capable of response times less than 20 seconds.

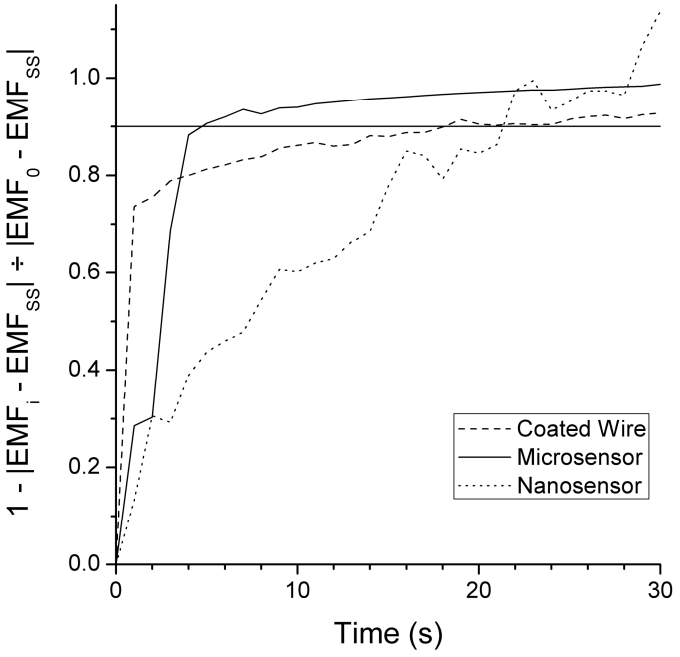

Fig. 2.6. A comparison of the fastest recorded response times for the CWE, micro-scale ISE, and nano-scale ISE configurations. These response times, defined as the time it takes the EMF of electrochemical cell to reach 90% of its final steady state value, were 18 s for the CWE, 11 s for the micro-scale ISE and 18 s for the nano-scale ISE.

Finally, the longevity of the solvent polymeric membrane for all three configurations was consistent with what was reported by Choi and Moon [7]. All three electrodes showed consistent response characteristics over a period of 61 days, with no appreciable loss in slope or LOD (data not shown).

2.6 Conclusions

We developed working nano- and micro-scale ISEs by applying solvent polymeric membrane to nano- and micropores made using MEMS fabrication techniques. We used an existing formulation for $HCrO_4^-$ selective solvent polymeric membrane to demonstrate our nano- and micro-scale ISEs exhibit similar slopes and LODs to a CWE configuration, making them useful as ISEs. From our additional investigation into the membrane formulation, we provided new selectivity coefficients for additional interferents, including $H_2PO_4^-$, F^-, CH_3COO^-, and SO_3^{2-}, with $\log_{10}$ values of −3.4, −3.4, −3.5, and −4.3, respectively. We also demonstrated an improved response slope of 61.7 ± 2.4 mV decade^{-1} and LOD of 3.03×10^{-6} M, elucidated the need for controlling the pH of sample, and showed the membrane formulation works consistently with lower ionophore content, even achieving a response slope of 50.7 ± 5.8 mV decade^{-1} and LOD of 4.34×10^{-6} M at 1 wt % ionophore. The nano- and micro-scale ISEs performed comparably to the CWE, giving response slopes of −65.2 ± 5.6 mV decade^{-1} and −58.6 ± 5.6 mV decade^{-1}, respectively; and LODs of 1.8×10^{-5} M and 2.1×10^{-5} M, respectively.

We used electrical resistance measurements to provide clear evidence of proper nano- and micropore formation and complete filling of the pores with solvent polymeric membrane, and indicated limits for potentiometric use of the sensors. The micro-scale ISE has a low enough resistance to be compatible with inexpensive potentiometers. The requirements for the nano-scale ISE are more in question, as our Axopatch 200 was not able to adequately measure its resistance properties. It is possible that the nano-scale ISE achieves a resistance of over 10 TΩ, but no performance loss was apparent when using our potentiometer with it, which has a 10 TΩ internal resistance.

We used AFM imaging to provide additional evidence of proper micropore formation and its complete filling with membrane, as well as to demonstrate that the surface area of the dried membrane exposed to sample exceeds that of the pore by 1.7 times. Our findings imply that our micro-scale ISEs are ideal for integration into micro channels, as they are relatively thin and smooth, protruding into the sample by only 250 nm at most. We found that AFM imaging was inadequate as a technique to image the nano-scale ISEs, since the membrane's size was on the order of surface features and smaller than dust particles on the chip surface.

Additionally, the nano- and micro-scale ISEs achieved excellent response times of 28.8 ± 6.1 s and 40.2 ± 25.4 s, respectively, which are comparable to those for conventional CWEs and make them very promising for future application in lab-on-a-chip technologies. Ultimately we conclude that both our nano- and micro-scale ISE fabrication techniques can bring miniaturized ISE technology that is relatively easy to work with to nano- and micro-scales. Considered together, these sensors offer vast engineering potential for lab-on-a-chip platforms that process analytes to form micro-scale or sub-micro-scale electrophoretic separation bands.

2.7 Acknowledgements

We thank Hajime Fuchida for improvement to our reference electrode fabrication protocol. We appreciate having graduate student support provided by an NIH-sponsored Biotechnology Training fellowship (D.R.). We would also like to thank the Washington State University School of Chemical Engineering and Bioengineering for their support.

2.8 References

1. D.E. Kimbrough, Y. Cohen, A.M. Winer, *et al.*, Critical Reviews in Environmental Science and Technology, 29 (1999) p. 1-46.

2. M. Gochfeld, Environmental Health Perspectives, 92 (1991) p. 3-5.

3. W.-P. Yang, Z.-J. Zhang, W. Deng, Analytica Chimica Acta, 485 (2003) p. 169-177.

4. E. Castillo, M. Granados, J.L. Cortina, Journal of Chromatography A, 963 (2002) p. 205-211.

5. R.C. Kamikawachi, M.M. Possetti, H.J. Kalinowski, *et al.*, Proceedings of SPIE-The International Society for Optical Engineering, 5622(*5th Iberoamerican Meeting on Optics and 8th Latin American Meeting on Optics, Lasers, and Their Applications*) (2004), 935-938.

6. I. Oehme O.S. Wolfbeis, Microchimica Acta, 126 (1997) p. 177-192.

7. Y.-W. Choi S.-H. Moon, Environmental Monitoring and Assessment, 92 (2004) p. 163-178.

8. A.K. Jain, V.K. Gupta, L.P. Singh, *et al.*, Talanta, 65 (2005) p. 716-721.

9. V.K. Gupta, A.K. Jain, P. Kumar, *et al.*, Sensors and Actuators B, 113 (2006).

10. M.A. Akl, A.K. Ghoneim, M.H.A. El-Aziz, Electroanalysis, 18 (2006) p. 299-306.

11. M.M. Ardakani, A. Dastanpour, M. Salavati-Niasari, Microchimica Acta, 150 (2005) p. 67-72.

12. M.B. Gholivand F. Sharifpour, Talanta, 60 (2003) p. 707-713.

13. A.K. Singh, A. Panwar, S. Kumar, *et al.*, Analyst, 124 (1999) p. 521-525.

14. Y.-W. Choi, N. Minoura, S.-H. Moon, Talanta, 66 (2005) p. 1254-1263.

15. E. Bakker E. Pretsch, Trends in Analytical Chemistry, 24 (2005) p. 199-207.

16. United States Environmental Protection Agency, Office of Water, EPA 816-F-03-016 (2003).

17. B. Jung, R. Bharadwaj, J.G. Santiago, Analytical Chemistry, 78 (2006) p. 2319-2327.

18. P.-A. Auroux, D. Iossifidis, D.R. Reyes, *et al.*, Analytical Chemistry, 74 (2002) p. 2637-2652.

19. G.J.M. Bruin, Electrophoresis, 21 (2000) p. 3931-3951.

20. B. Zhang, H. Liu, B.L. Karger, *et al.*, Analytical Chemistry, 71 (1999) p. 3258-3264.

21. F. Baldessari J.G. Santiago, Journal of Nanobiotechnology, 4 (2006) p. 12.

22. B. Liu, D. Rieck, B.J.V. Wie, *et al.*, Biosensors & Bioelectronics, Accepted (2008).

23. M.A. Plesha, B.J.M. Van Wie, James M., D.A. Kidwell, Analytica Chimica Acta, 570 (2006) p. 186-194.

24. R. Koncki, S. Glab, A. Hulanicki, Analytica Chimica Acta, 273 (1993) p. 477.

25. G. Mori M. Giannetto, Ann. Chim. (Rome), 89 (1999) p. 601.

26. F.J.S.d. Viteri D. Diamond, The Analyst, 119 (1994) p. 749.

27. R.P. Buck E. Lindner, Pure & Applied Chemistry, 66 (1994) p. 2527-2536.

28. Y. Umezawa, P. Bühlmann, K. Umezawa, *et al.*, Pure & Applied Chemistry, 72 (2000) p. 1851-2082.

29. E. Bakker, P. Bühlmann, E. Pretsch, Chemical Reviews, 97 (1997) p. 3083-3132.

30. W.S. Gibbons R.P. Kusy, Thermochimica Acta, 284 (1996) p. 21-45.

31. R.K. Tandon, P.T. Crisp, J. Ellis, *et al.*, Talanta, 31 (1984) p. 227-228.

32. S. Mathison E. Bakker, Analytical Chemistry, 70 (1998) p. 303-309.

33. T. Sokalski, A. Ceresa, T. Zwickl, *et al.*, J. Am. Chem. Soc., 119 (1997) p. 11347-11348.

34. O.A. Seppänen, W.J. Fisk, M.J. Mendell, Indoor Air, 9 (1999) p. 226-252.

35. J. Wang, C.D. Meyers, G.A. Robertson, J. Gen. Physiol/, 115 (2000) p. 749-758.

36. J.E. Hall, The Journal of General Physiology, 66 (1975) p. 531-532.

37. M. Aguilella-Arzo, V.M. Aguilla, R.S. Eisenberg, Eur Biophys J, 34 (2005) p. 314-322.

38. P. Vanýsek, in: D.R. Lide, Editor(Ed.), CRC Handbook of Chemistry and Physics, CRC Press, Cleveland, OH, 2007/08, p. 5-75.

39. P. Vanýsek, in: D.R. Lide, Editor(Ed.), CRC Handbook of Chemistry and Physics, CRC Press, Cleveland, OH, 2007/08, p. 5-77.

40. B. Fozard, R.P. Sheldon, P.C. Wright, Journal of Applied Polymer Science, 22 (1978) p. 1167-1176.

CHAPTER 3
FUTURE WORK

Our proof of concept for miniaturized ISEs is a major step forward for our lab, but it is only one step in a larger process we have envisioned that is capable of solving the problem of adapting ISE technology to monitoring trace level analytes in real world samples. Our design rationale is that integrating miniaturized ISEs, trace-level ISE design, lab-on-a-chip preconcentration and preseparation technology, and strong engineering approaches to working with real world samples (such as dealing with analyte sorption) will increase the linear range and usefulness of ISEs and eliminate the major problem of their limited selectivity to an extent that will make the technology attractive and reliable enough to be adopted for use in current practice. The scope of this work was to target the ISE miniaturization step, while fitting it into the context of our overall vision. Hence our goal was to develop a successful fabrication process for producing miniaturized ISEs, such that they could be taken to the next phase of our design plan, which is integrating miniaturized ISEs into lab-on-a-chip preseparation and preconcentration technology.

Overall the manuscript shows that both the nano- and micro-scale ISEs are ready for moving forward, exhibiting nearly identical performance to our CWE configuration. The morphology characteristics of the micro-scale ISE demonstrate it is ideal for microchannel integration and imply that the nano-scale ISE is as well, but additional imaging is recommended using a different technique than AFM whereby nano-scale ISE membrane morphology can be conclusively determined. One possible technique is environmental SEM, which could be used without sacrificing the sensor.

At this point, there are two full steps next in the design rationale that can be conducted in parallel. The first step is threefold: 1) we integrate the micro-scale ISEs into a micro-scale ITP process and demonstrate its ability to accurately measure analyte concentrations under controlled conditions, 2) we do the same for a nano-scale ISEs integrated into a nano-scale ITP process, and 3) we construct a larger, more powerful, and complex ITP separation scheme using both micro-scale and nano-scale steps. The experimental work for this overall process has already begun in our lab, as we so far have achieved over 31x preconcentration with full preseparation of a chromate sample in artificial seawater media. The second step is twofold: 1) we calibrate more miniaturized ISEs for targeting our desired analytes, and 2) we enhance the miniaturized ISE technology by integrating cutting edge ISE fabrication techniques to render the miniaturized ISEs capable of nanomolar detection and greatly improved selectivity coefficients. We expect that the major hurdles in these stages of our design rationale will be centered on successful engineering of the devices. For example, there are difficulties associated with combining miniaturized ISEs and ITP, which are both electrically dependent processes; and novel electrochemical cell designs will have to be crafted for existing membrane formulations that have not been adapted to trace-level analysis, each instance of which is a publishable paper. This step would break new ground for our lab.

The final step will be a proof-of-concept study where we build a prototype trace-level heavy metals monitoring device, combining trace-level ISEs and ITP preconcentration and preseparation with engineering approaches to overcoming the challenges presented by introducing real world samples into the system. Major challenges will be: 1) to prevent contamination and fouling of the ITP flow channels, 2) finding reliable and consistent techniques to remove complexing agents from bound ions, 3) designing an efficient and watertight footprint

for the overall device, 4) designing onboard software for the device and 5) designing a means for interfacing with the device to download and analyze data. This final step constitutes a major undertaking, and may have to be split into sub-projects to be successful. It completes our design rationale, which if successful could lead to a marketable commercial product that has the potential to revolutionize the regulatory industry. If fully realized, instead of relying on grab-sampling and ICP-MS, coastal managers could take a continuous monitoring device into the field with femtomolar sensitivity, capable of monitoring multiple species at once, and costing from $500-$1000 for initial capital investment and < $50 for quarterly maintenance costs based on our estimates. Given these possibilities, even a more conservative realization of this device is extremely attractive.

Ultimately, the overall success of this project is not merely found in the successful fabrication and demonstration of miniaturized ISEs, but the research course that could springboard off the published manuscript. In addition to revolutionary trace-level monitors, more possibilities come to mind: lab-on-a-chip immunosensing using miniaturized ISE technology; bioreactor feedback control through miniaturized ISEs; and clinical applications involving miniaturized trace-level ISEs. The possibilities from this point are numerous and promising, offering additional research projects for years to come with considerable potential for technology transfer and positive societal impact.